PERGAMON International Journal of Impact Engineering 29 (2003) 95–104

INTERNATIONAL JOURNAL OF IMPACT ENGINEERING

www.elsevier.com/locate/ijimpeng

Behind Armor Debris Investigation (Part II)

Werner Arnold*, Ernst Rottenkolber**

*TDW Gesellschaft für verteidigungstechnische Wirksysteme mbH, Hagenauer Forst, D-86529 Schrobenhausen, Germany;

**CONDAT Gesellschaft für EDV-Consulting und Datentechnik mbH, Maximilianstr. 28, D-85298 Scheyern-Fernhag, Germany;

Abstract

On the occasion of the latest HVIS Symposium 2000 in Galveston, TX, the first part of the Behind Armor Debris (BAD) investigation was presented [1]. The secondary fragments were caused by shaped charge jet impact (caliber 115 mm) on a armor steel plate. Besides the influence of the overmatch and of a polyethylene liner on the BAD cloud under 0° NATO obliquity angle, first applications to the German Tank Vulnerability Model (PVM) were demonstrated.

The second part of the study covers measurements of the velocity and mass distribution within the debris cloud as a function of the significant parameters overmatch, liner thickness and obliquity angle. The 0° NATO firings of the first part were completed by firing tests under 60° NATO. One result we found out was, that the BAD cloud is hollow, i.e. the secondary fragments are concentrated on a thin skin.

The evaluation of the extensive test matrix including the mass determination out of the fragment hole distribution in the witness plate was carried out with a novel method, which will be described here in more detail. Consequently, the applied ellipsoid model completely characterizes the BAD cloud within the mentioned range of the significant parameters. The trends observed are described. All results were filed in a comprehensive ACCESS database, which is now the basis for the PVM ellipsoid model. The BAD cloud is thus represented realistically and the damage caused by secondary fragments can be simulated as accurately as possible.

© 2003 Elsevier Ltd. All rights reserved.

Keywords: Behind Armor Debris (BAD), Shaped Charge Attack, Overmatch, Target Liner, Obliquity Angle, Vulnerability

1. Introduction

The present paper completes an extensive study of the creation of secondary fragments when shaped charges (SC) are fired against armor steel targets. The purpose of the investigation was to enable a better and more precise simulation of the secondary fragment effects for an application in the German tank vulnerability model PVM. To achieve this, it was necessary to know how the secondary fragments depend on the significant parameters. To accumulate these data, a number of firing tests were carried out using a 115 mm caliber high precision shaped charge. Parameters varied in the experimental program were the obliquity angle, the overmatch, (defined as OM = 1-P/P_0, P = target thickness, P_0 = SC-penetration into semi-infinite target) and finally, the thickness

0734-743X/$ - see front matter © 2003 Elsevier Ltd. All rights reserved.
doi:10.1016/j.ijimpeng.2003.09.009

of the polyethylene (PE) liner. For statistical reasons, at least three firing tests were performed for each fixed set of parameters. Together with the extra measurements of the velocity distribution, this resulted in a test matrix based on about 100 SC firings.

The first part of this work was already presented at the HVIS 2000 symposium [1]. The results achieved with varying overmatch OM and PE liner thickness dL at an obliquity angle of 0° NATO were described. The influence of these two parameters was investigated and the effects of the obtained BAD cloud description were simulated in the tank vulnerability model PVM.
Now, the results are extended by the obliquity angle variation. Before this, we discuss the velocity distribution of the secondary fragments within the BAD cloud, which was determined experimentally and subjected to a numerical simulation. In addition, we sketch a novel data reduction method that replaces the time consuming counting of the fragment impacts by a computerized process. This method also permits to obtain the mass and angle distribution inside the BAD cloud based on the distribution of the impact holes at the witness plates. Having determined the velocity, direction and mass of the secondary fragments, the parameters of the BAD ellipsoid are completely known. Finally, we show a series of hole distributions in the witness plates to discuss the observed dependencies of the secondary fragment distribution on the significant parameters.

The experimental results obtained in this work, form the basis of a more accurate analysis of secondary fragment effects in the tank vulnerability model PVM. The underlying formalism is called the "ellipsoid model", a name motivated by the assumed shape of the BAD cloud. The X-ray shadowgraph shown in Fig. 1 clearly supports this assumption.

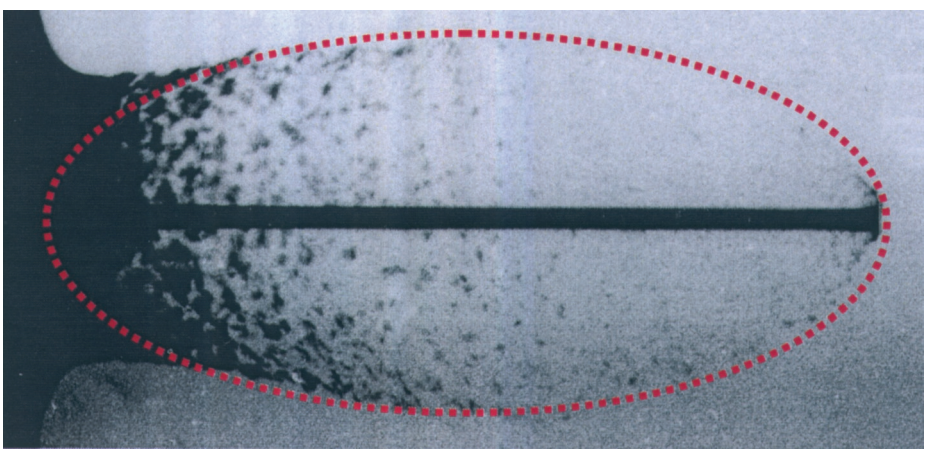

Fig. 1. Ellipsoid model for the BAD cloud.

2. Velocity Distribution of Bad Cloud

In addition to the mass and angle distribution of the secondary fragments, the velocity distribution represents the third essential quantity in determining the BAD cloud. Knowledge of the velocity of the fragments is also necessary for the calculation of fragment masses from hole sizes, a topic we will discuss later again. The test set-up followed the one defined in [1] with the exception, that a slit shield captured the major BAD cloud portion, admitting the passage of fragments in the vicinity of the measurement plane only (Figure 2). That means an ellipse is cut out of the BAD ellipsoid. The fragments within the ellipse were recorded on the X-ray film with two X-ray flashes triggered after pre-defined, adjusted time delays.

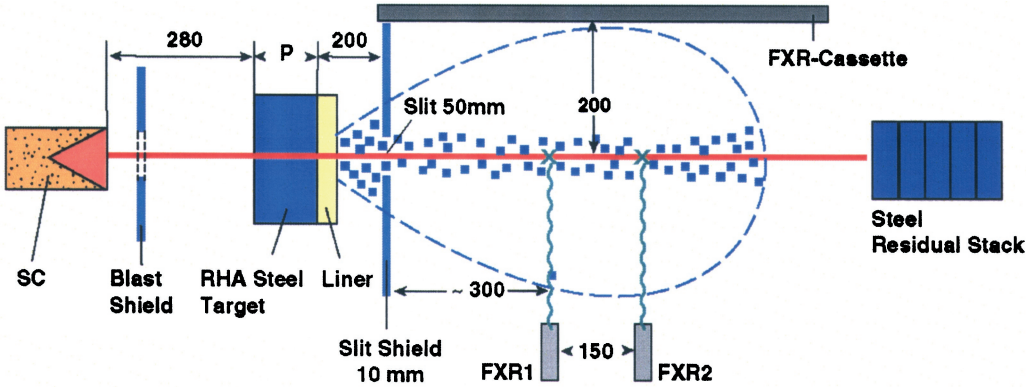

Fig. 2. Test set-up: BAD velocity measurement with slit shield.

The tests started under a 0° NATO obliquity angle. Subsequent to this, the measurements under 60° NATO obliquity angle were carried out. For these tests, the film cassette had to be shifted to account for the BAD cloud's deflection from the firing axis. The velocity distributions for the various overmatches OM and liner thicknesses dL were determined this way. A fully evaluated result for the parameter set OM = 0.8, dL = 0 mm and $\theta = 0°$ NATO (Test No. 53863) is presented as an example in Figure 3. The X-ray trigger times were 130 µs and 140 µs, the corresponding particle positions are displayed as a cross or a circle. A turned cross and square are used to indicate the position of the jet tip particle that moves ahead. The origin of the coordinate system coincided with the perforation spot on the target rear side, i.e. the virtual source of the secondary fragments. A blast shield was arranged in front of the shaped charge. The velocity vectors were calculated from the positions at the trigger times.

All of the fragment particles that can be resolved on the X-ray picture are concentrated on the surface of the elliptical area. A dashed line ellipse provides the circumference of the ellipsoid in the measurement plane. Its length/diameter ratio is about L/D = 2.

The fragment ellipsoid head velocity was about 90 % of the jet tip velocity. The minimum ellipsoid velocity was defined to be 1400 m/s. Given the velocity bounds and the L/D-ratio, the radial velocity of a fragment can be determined. The majority of holes in the witness plates was caused by these fast secondary fragments, the so-called "erosion fragments". The few bigger holes were generally due to fragments with a mass greater than 2 g, having lower velocities (200 – 1400 m/s). These fragments were called "ring fragments", since they originate from an annular region around the penetration channel at the rear side of the target. With test conditions differing from that of Fig. 3, similar results were observed. In addition, the experimental findings could be supported by OTI*HULL code simulations. Figure 4 shows snapshots from a simulation, indicating that the debris cloud produced by a continuous shaped charge jet indeed resembles an ellipsoid that is not filled with secondary fragments.

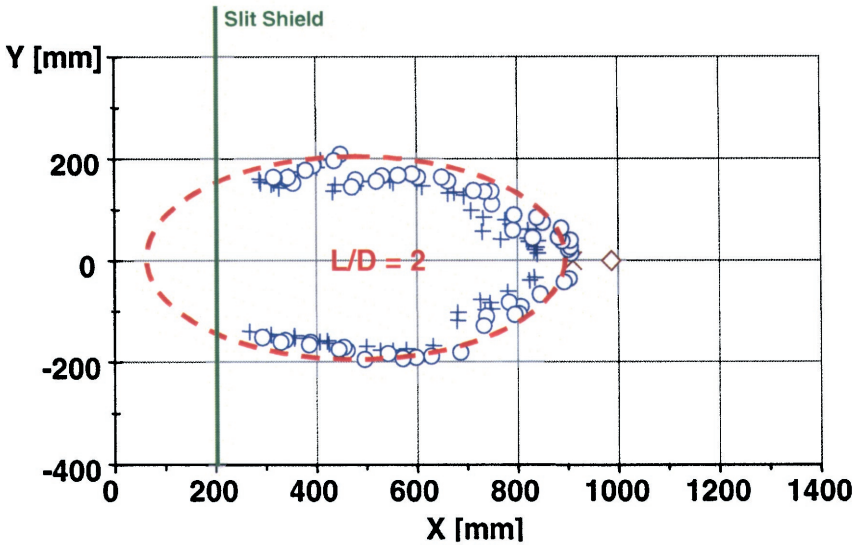

Fig. 3. Velocities of fragments were determined from position and time measurements based on double exposure X-ray shadowgraphs.
(Test No. 53863, OM = 0.8, dL = 0 mm, θ = 0° NATO, t_1 = 130 μs, t_2 = 140 μs)

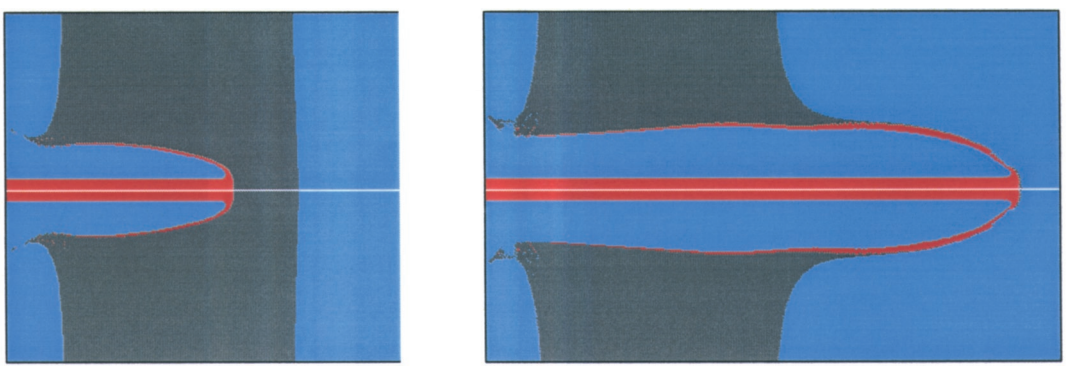

Fig. 4. HULL simulation of hypervelocity projectile impact. The mushroom region behind the erosion front develops into the debris ellipsoid. Fragments are concentrated at the surface of the ellipsoid.

Table 1 summarizes the results of the velocity measurement at θ = 0° NATO with OM = 0.2 to 0.8. These values were also observed for θ = 60° NATO with the difference that the ellipsoid is deflected off the firing axis.

Table 1. Velocity measurement, fragment ellipsoid (θ = 0° NATO)

OM	0.2	0.4	0.6	0.7	0.8
v_{max} [mm/μs]	2.9	3.6	4.9	5.4	6.3
v_{min} [mm/μs]	1.4	1.4	1.4	1.4	1.4
v_{rad} [mm/μs]	0.4	0.6	0.9	1.0	1.2

3. Test Setup and Test Matrix

The test set-up for the 60° NATO firings was almost identical with the one used for the 0° NATO firings [1]. The only differences were that not only the targets were inclined to 60° NATO but correspondingly also the 0.5 mm mild steel witness plates to 30° NATO to cope with the BAD cloud deflection expected to be $\theta/2 = 30°$ NATO. The perpendicular distance between the target and the witness plate was again 990 mm.

Contrary to [1], the evaluation of the witness plates was carried out with a new process described in the following section. With this time saving automated method, also the BAD fragment masses can be determined, therefore, the 0° NATO trials were re-evaluated. Concerning the number of fragments, correlating with the results obtained with manual counting could validate the process. With the 100 firing tests, the following parameter range was covered:

- $\theta = 0°, 60°$ NATO
- OM = 0.2, 0.4, 0.6, 0.7, 0.8
- dL (PE) = 0, 20, 30, 50 mm
- Velocity distribution in the BAD ellipsoid

4. Novel Evaluation Method

The perforated witness plates were painted black on the impact side and subsequently placed in front of an area light source with the other side and photographed. On the film, these holes are visible as bright light spots. Since due to optical effects (e.g. diffraction), these measured light spots are bigger than the real holes, a calibration was carried out in advance.

Circular holes of 1 mm to 35 mm diameter were drilled into a witness plate. This plate with the hole mask was also photographed and evaluated. In addition, the exposure process was optimized on this occasion by varying certain parameters like exposure time, aperture, distances, light sources etc. The photo of this hole mask was scanned and read into a PC to be evaluated with a self-developed image analysis software. Working with $2^8 - 1 = 255$ gray scales per pixel allowed identification of the hole edge with an accuracy sufficient to detect and analyze holes as small as 0.5 mm diameter. Figure 5 shows a calibration curve elaborated this way. The inserts show the hole mask and the way in which a pre-defined threshold value for the gray scale exerts influence on the hole size measured.

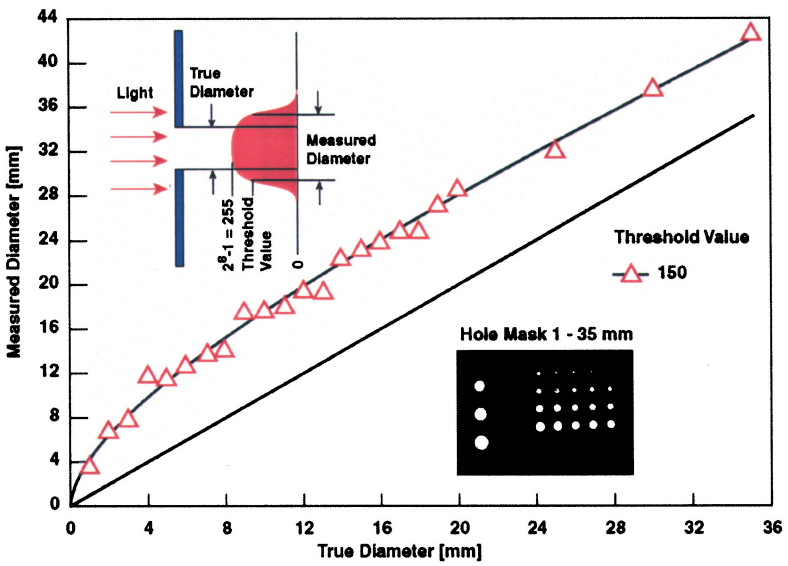

Fig. 5. Hole calibration using a hole mask.

For all of the witness plates analyzed, the same process was applied without variation of any parameter so that the evaluations are consistent with each other. Figure 6 shows the scanned photo of the two 1 x 2 m² witness plates on the left side and the corresponding computer evaluation on the right side (Test No. 53634, OM = 0.8 dL = 0 mm, θ = 0°). All hole data like coordinates, hole length, width and orientation angle were stored in an ACCESS database.

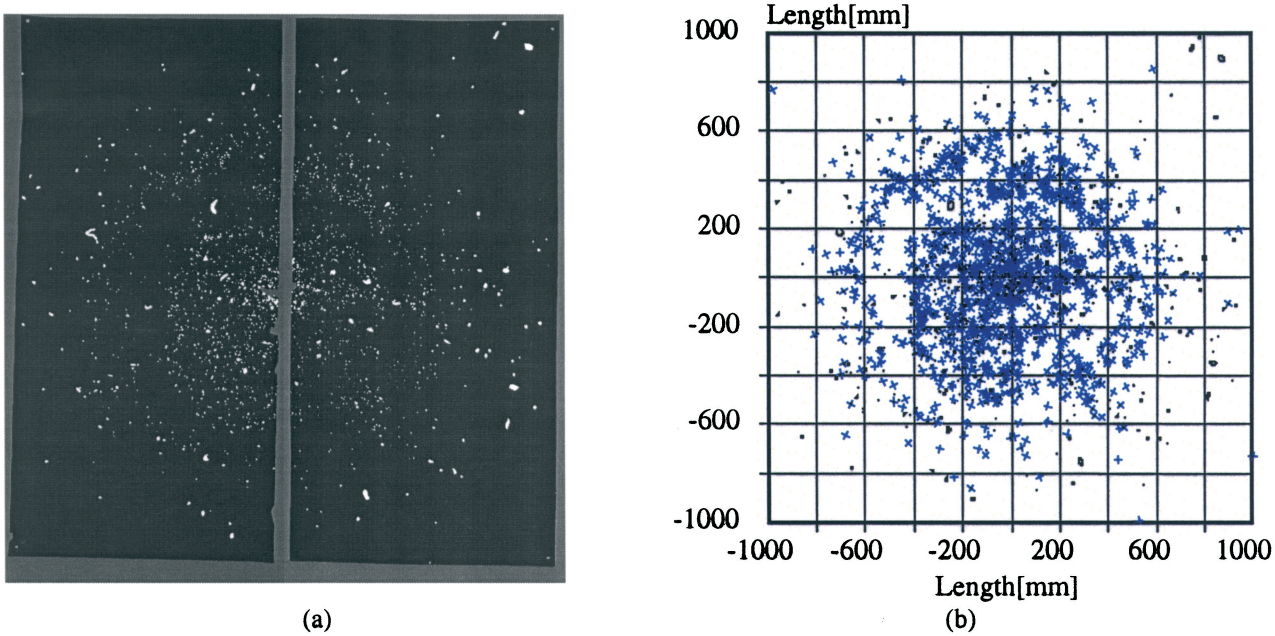

Fig. 6: The photo showing the witness plates (a) and the diagram showing the computer evaluation (b) (Test No. 53634, OM = 0.8 dL = 0 mm, θ = 0°).

The second part of the developed software reads these recorded data and permits assignment of the fragments into concentric rings, as in [1], so that on its turn, the fragment distribution can be presented as a function of the emission angle. In addition, the fragment mass is derived on the basis of the hole size and the corresponding fragment velocity. The individual steps of this process are described in [2].

Among others, the following is considered in this context:

- Dependence of the hole size on the impact velocity
- Fragment orientation
- Fragment shape relative to a shape factor of the hole

The required assignment of fragment hole and fragment velocity is unambiguous since the measured fragment ellipsoid is empty and the fragments are concentrated at the surface only. Figure 7 comprises an example evaluation with cumulative number of fragments, hole area and fragment mass as a function of the emission angle for test No. 53634 shown in Figure 6.

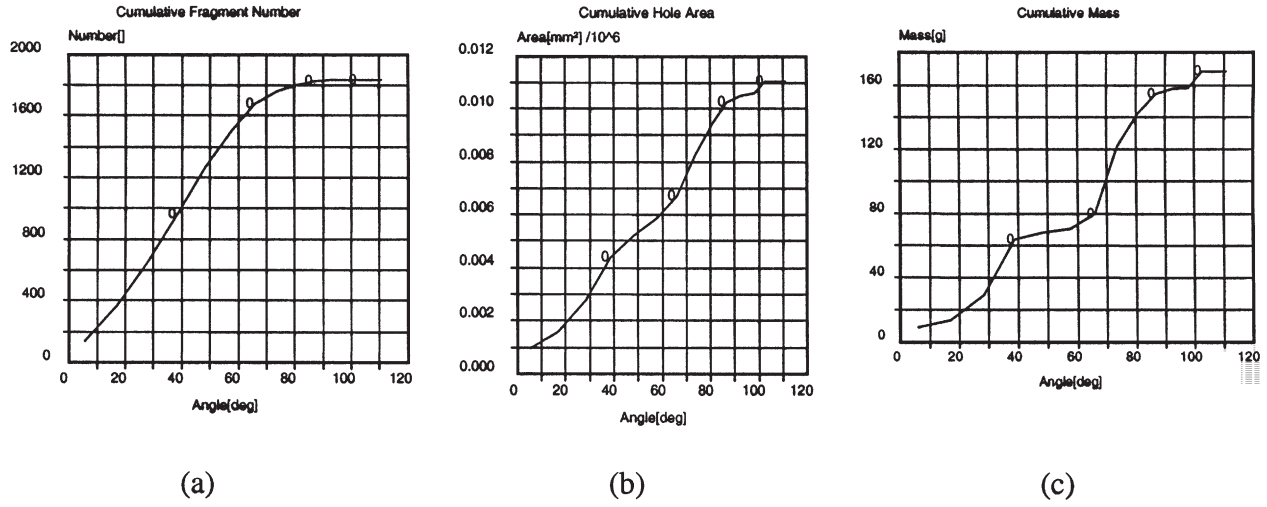

Fig. 7. Cumulative number of fragments (a), hole area (b) and fragment mass (c) as a function of the emission angle (Test No. 53634 of Figure 6).

For the vulnerability model PVM, mass and angle distributions of the BAD cloud are required in analytical form. The PVM model distributions are fitted to the measured curves. For the test presented, such a mass distribution fit is illustrated in Figure 8. At very small fragment masses, deviations from the fit curve occur, probably because the smallest mass particles are not capable of perforating the 0.5 mm plate. There is an innumerate quantity of very little craters on the witness plate. This portion in small masses is considered via the theoretical distribution curve. The smallest masses that could be resolved experimentally correspond to ballistically estimated mass limits at the high velocities for a 0.5 mm plate. Together with the directly measured hole data the derived fragment data and distribution parameters were also stored in the ACCESS database and made available for further analysis.

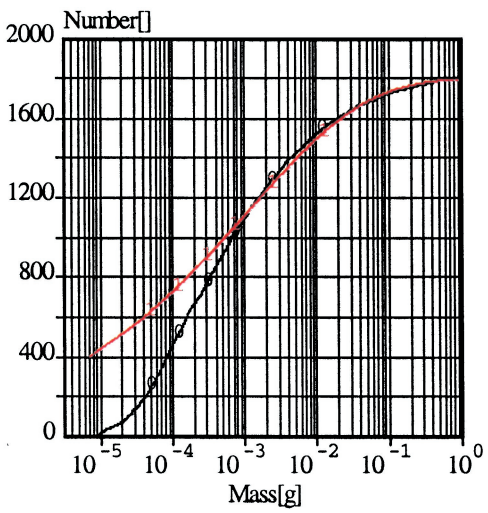

Fig. 8. Measured (0) and fitted (1) mass distribution of the BAD cloud (Test No. 53634).

5. Results

The results of the firing trials are presented hereafter with respect to the observed trends regarding the above significant parameters:

- Obliquity angle
- Overmatch
- Liner thickness

These trends are visualized most clearly with elucidating example photos of witness plates subjected to firing attacks. Therefore, these photos represent the basis of discussion.

5.1 Obliquity Angle

The two extreme values $\theta = 0°$ and $\theta = 60°$ NATO were investigated to cover the relevant range of obliquity angles. Corresponding witness plates for OM = 0.8 and dL = 0 mm are compared to each other in Figure 9. At 0°, the firing axis is in the center of the plate (the 2 x 2 m² plate is composed of two 1 x 2 m² plates) and at 60° it is in the center of the top half (430 mm underneath the plate's upper edge).

At 0° the fragment impacts are distributed symmetrically around the firing axis, while at 60°, a deflection from the firing axis occurs. The center of the fragment cloud shows lower deflection with rising overmatch and reaches about $\theta/2 = 30°$ under an OM = 0.8. At 60° more fragments are produced. In the presented example of Figure 9, a cumulative number of about 1800 fragments results at 0° while the cumulative number is approximately 2350 fragments at 60°. This is, however, understandable, as more and more eroding material is involved on the target's rear side with increasing angle.

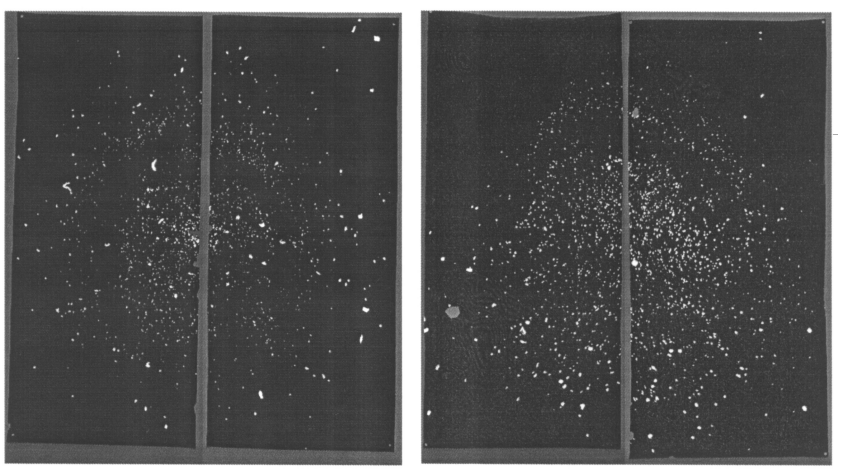

 # 53634
0° NATO

 # 53935
60° NATO

Fig. 9: Witness plates at 0° NATO and 60° NATO obliquity angle with OM = 0.8 and dL = 0 mm.

5.2 Overmatch

In [1] it was already observed that at 0° NATO the number of fragments increases considerably with rising overmatch as well as the emission angle rises. This trend could be confirmed at 60° NATO, with the deflection of the BAD cloud away from the firing axis already mentioned.

Figure 10 comprises an exemplary presentation of the witness plates used for firing attacks under θ = 60° and dL = 0 mm. The overmatch rises from left to right as OM = 0.2, 0.6 and 0.8.

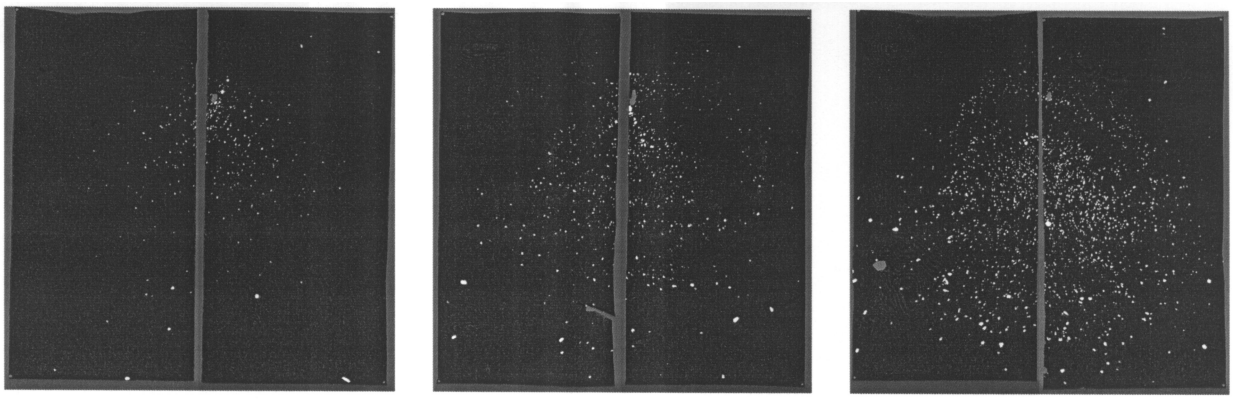

Fig. 10: Witness plates for OM = 0.2, OM = 0.6 and OM = 0.8 with θ = 60° and dL = 0 mm.

5.3 PE Liner Thickness

Finally, the effect of the PE liner thickness is discussed. Once again, dependences at 0° NATO became apparent in [1]. With increasing liner thickness, the number of fragments decreased and concurrently the remaining fragments were increasingly focused into smaller emission angles. This trend was confirmed, too, at 60° NATO with the only exception that the fragment cloud is deflected from the firing axis, as mentioned before.

Figure 11 presents example witness plates, from left to right: dL = 0 mm, dL = 20 mm and dL = 50 mm. Both effects described above are clearly demonstrated. Another phenomenon can be recognized. The BAD cloud is deflected from the firing axis while the angle of deflection for the center of the fragment cloud approaches a value of about θ/2 = 30° with increasing overmatch. A certain fragment portion from the vicinity of the jet however, is not influenced by this deflection and is somehow dragged with the jet. This can be seen especially well on the right witness plate of Figure 11 with dL = 50 mm.

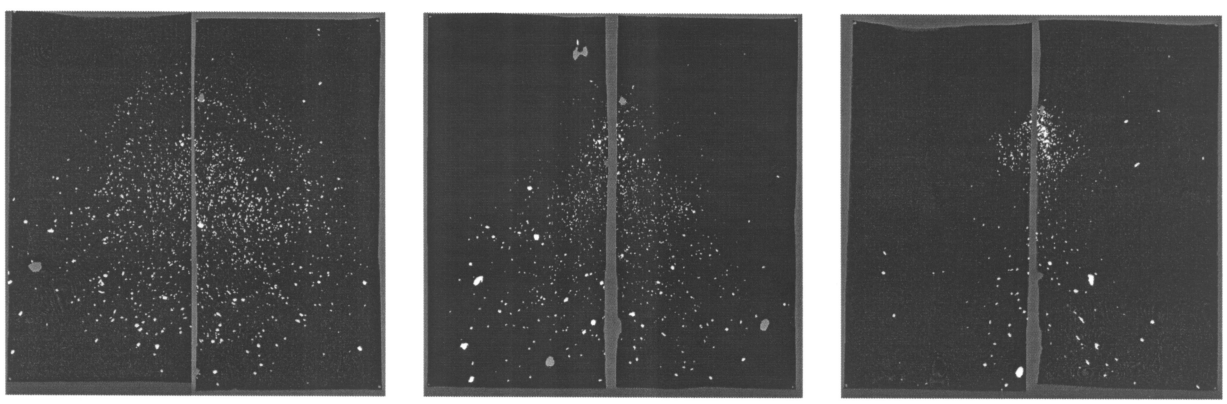

Fig. 11: Witness plates for dL = 0 mm, dL = 20 mm and dL = 50 mm with OM = 0.8, θ = 60°.

6. Conclusions

An extensive investigation of secondary fragments generated by shaped charge attack was performed. In the course of the study, approximately one hundred tests with a 115 mm caliber shaped charge were performed. The following parameter range was covered with this test matrix:

- $\theta = 0°, 60°$ NATO
- OM = 0.2, 0.4, 0.6, 0.7, 0.8
- dL (PE) = 0, 20, 30, 50 mm
- Velocity distribution inside the BAD ellipsoid

A new method to evaluate the witness plates subjected to firing attacks permitted – besides automated evaluation - to determine the mass and angle distribution of the debris cloud. Using the velocity distribution, all parameters of the ellipsoid model could be determined in this way. The complete information was stored in an ACCESS database and made available for use in the updated tank vulnerability model PVM. The trends in the behavior of the BAD cloud with respect to the relevant parameters listed above were described.

Acknowledgement

This paper was elaborated by TDW for the German Federal Office of Defense Technology and Procurement (Bundesamt für Wehrtechnik und Beschaffung) under the contract No. E/W21F/0A055/X5109. TDW would like to express its thanks to CONDAT GmbH for its contributions.

References

[1] Arnold W, Paul W. Behind Armor Debris Investigation and their Application into a New Vulnerability Model *Int. J. of Impact Engng.*, 2001; **26**: 21-32

[2] Rottenkolber E. A PC Program to Analyze Secondary Fragment Distributions *CONDAT-Report CB 100005,* 2000